Polymers **2014**, *6*, 926-948; doi:10.3390/polym6030926

OPEN ACCESS

polymers

ISSN 2073-4360

www.mdpi.com/journal/polymers

Article

Strong Screening Effect of Polyhedral Oligomeric Silsesquioxanes (POSS) Nanoparticles on Hydrogen Bonded Polymer Blends

Chin-Wei Chiou [1], Yung-Chih Lin [1], Lei Wang [2], Chiharu Hirano [2], Yoshinori Suzuki [2], Teruaki Hayakawa [2] and Shiao-Wei Kuo [1,*]

[1] Department of Materials and Optoelectronic Science, Center for Functional Polymers and Supramolecular Materials, National Sun Yat-Sen University, Kaohsiung 804, Taiwan; E-Mails: m023100011@student.nsysu.edu.tw (C.-W.C.); d993100007@student.nsysu.edu.tw (Y.-C.L.)

[2] Department of Organic and Polymeric Materials, Tokyo Institute of Technology, 2-12-1-S8-36 O-okayama, Meguro-ku Tokyo 152-8552, Japan; E-Mails: wang.l.ag@m.titech.ac.jp (L.W.); hirano.c.ab@gmail.com (C.H.); suzuki.y.bd@gmail.com (Y.S.); hayakawa.t.ac@m.titech.ac.jp (T.H.)

* Author to whom correspondence should be addressed; E-Mail: kuosw@faculty.nsysu.edu.tw; Tel./Fax: +886-7-525-4099.

Received: 21 February 2014; in revised form: 12 March 2014 / Accepted: 17 March 2014 / Published: 21 March 2014

Abstract: In this study we used anionic living polymerization to prepare two different homopolymers: a poly(methyl methacrylate) (PMMA) and a PMMA derivative presenting polyhedral oligomeric silsesquioxane (PMA-POSS) units as its side chains. We then employed differential scanning calorimetry (DSC), Fourier transform infrared (FTIR) spectroscopy, and wide-angle X-ray diffraction (WAXD) to investigate the miscibility and specific interactions of PMMA and PMA-POSS with three hydrogen bonding donor compounds: poly(vinyl phenol) (PVPh), phenolic resin, and bisphenol A (BPA). DSC revealed that all of the PVPh/PMMA, phenolic/PMMA, and BPA/PMMA blends exhibited a single glass transition temperature, characteristic of miscible systems; FTIR spectroscopic analyses revealed that such miscibility resulted from hydrogen bonding interactions between the C=O groups of PMMA and the OH groups of these three hydrogen bonding donor compounds. In contrast, all of the PVPh/PMA-POSS, phenolic/PMA-POSS, and BPA/PMA-POSS blends were immiscible: DSC revealed two

glass transition temperatures arising from strong screening effects (FTIR spectroscopy) and high degrees of aggregation (WAXD) of the POSS nanoparticles. We propose that the value of the intramolecular screening effect (γ) should be very close to 1 for all PMA-POSS blend systems when POSS nanoparticles appear as the side chains of PMMA, such that the OH groups of the hydrogen bonding donor compounds cannot interact with the C=O groups of PMA-POSS.

Keywords: miscibility; hydrogen bonding; POSS; screening effect

1. Introduction

Polymer blending can be a powerful route toward materials exhibiting properties and cost performances superior to those of their individual components. To enhance the formation of single-phase, miscible polymer blends, it is necessary to ensure the presence of favorable and specific intermolecular interactions (e.g., hydrogen bonding, ion–dipole, π–π, and charge transfer interactions) [1–5]. The blending of poly(methyl methacrylate) (PMMA, a hydrogen bond acceptor polymer) with various hydrogen bond donor polymers, including poly(vinyl phenol) (PVPh) and phenolic resins, has been investigated widely over the years [6–12]. These systems generally form miscible blends as a result of intermolecular hydrogen bonding interactions between the C=O groups of PMMA and the OH groups of the hydrogen bond donor polymers [11–15]. The miscibility of polymer blends is commonly ascertained through the use of differential scanning calorimetry (DSC) to measure glass transition temperatures (T_g). Moreover, Fourier transform infrared (FTIR) spectroscopy has been a powerful tool for characterizing the detailed structures of polymers and their specific interactions, which affect local electron densities and, thereby, result in frequency shifts [16–18].

Painter and Coleman association model (PCAM) is modified by the Flory-Huggins theory to include a free energy change associated with hydrogen bonding that has both entropic and enthalpic contribution ($\Delta G_H/RT$). Furthermore, the inter-association equilibrium constant and its related enthalpy necessary to quantify this free energy can be calculated at various temperatures by FTIR according to PCAM [1]. Serman *et al.* [11] used DSC to study the phase behavior of PVPh blended with PMMA, finding them to be miscible; they determined the inter-association equilibrium constant (K_A) for the interactions of the OH groups of PVPh with the C=O groups of PMMA to be 37.4. Painter and Coleman proposed [19–21] that "intramolecular screening and functional group accessibility" can have significant effects on the number of hydrogen-bonded functional groups. They used FTIR spectroscopy to measure the fraction of hydrogen-bonded C=O groups present in miscible blends of PVPh/PMMA as functions of the composition and temperature and compared their results with those of analogous PVPh-*co*-PMMA copolymers and polymer solutions of PVPh and ethyl isobutyrate (EIB) [22]. Painter and Coleman found that there were significant differences in the equilibrium fractions of intermolecular hydrogen-bonded C=O groups that formed under otherwise identical concentrations and temperatures [22]. They introduced an intramolecular screening parameter (γ), defined as the fraction of same-chain contacts originating from polymer chain self-bending, primarily through local, but also through long-range, connectivity effects [19–21]. Painter and Coleman also examined the screening

effect for a hyperbranched, dendrimer-like polyester in the presence of low-molecular-weight PVPh as a model compound. The values of γ for a linear chain structure blend (e.g., PVPh/PMMA) is approximately 0.3; for a dendrimer-like polyester blend (e.g., PVPh/dendrimer-like polyester) it is approximately 0.8 [19,23].

Scheme 1. Synthesis of PMMA and PMA-POSS homopolymers through living anionic polymerization.

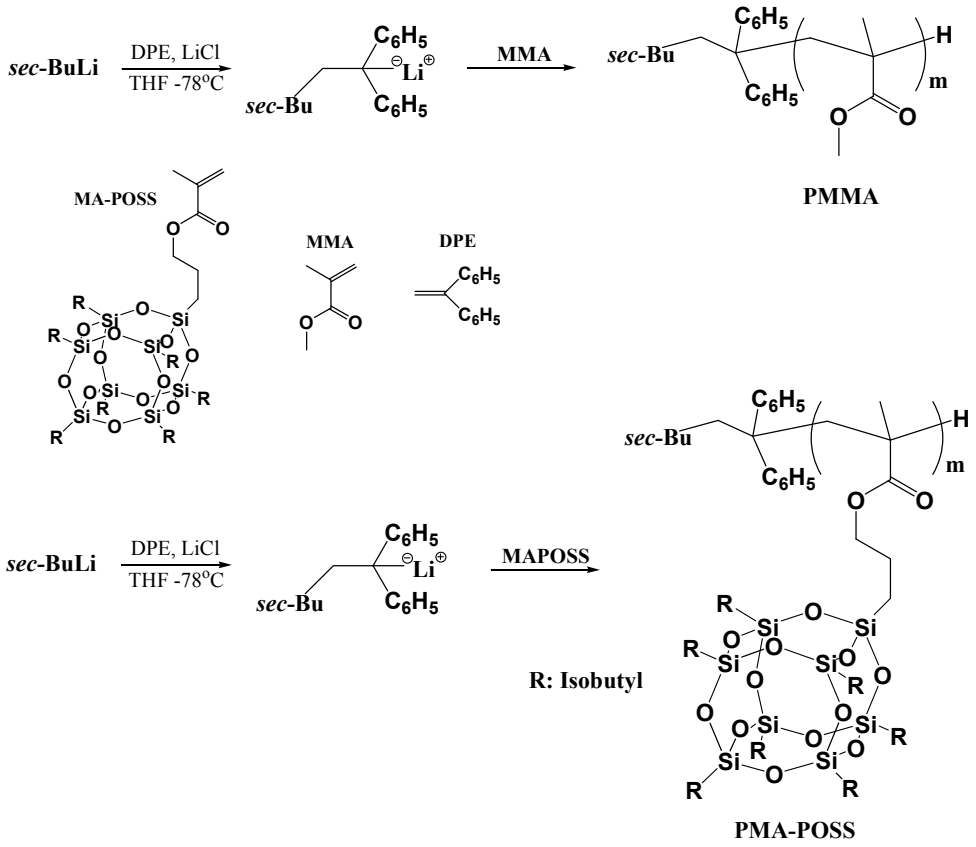

Phenolic/PMMA systems are also miscible blends that have been studied extensively [24,25]. In a previous study, we determined a value of K_A of 20 directly through a least-squares fitting procedure based on the fraction of hydrogen-bonded C=O groups measured experimentally in a binary phenolic/PMMA blend [25]. We also used atom transfer radical polymerization (ATRP) to prepare inorganic/organic polymer hybrids featuring polyhedral oligomeric silsesquioxane (POSS) moieties at the chain ends; we obtained well-defined PMMA and PMMA-POSS homopolymers with designed molecular weights (*ca.* 40,300 and 38,300 g/mol) and then blended them with phenolic resin. POSS is a new type of material capable of forming various nanocomposites [25]. POSS derivatives are interesting materials because one or more of their organic groups can be functionalized for polymerization, while their remaining unreactive groups can be designed to solubilize the inorganic core and control the interfacial interactions between the POSS units and the polymer matrix. Due to their potential for advanced performance (e.g., high thermal stability; low flammability; low dielectric constant; low surface energy) relative to nonhybrid counterparts, POSS–polymer hybrid materials have attracted great interest recently [26–35]. We observed a "screening effect" in phenolic/PMMA-POSS blends arising from the tethered POSS units at the chain ends, with the inter-association equilibrium

constant for the interactions of the OH groups and POSS units being greater than that of the OH and C=O groups [25]. The value of γ of 0.65 for the phenolic/PMMA-POSS blend was lower than that for the dendrimer-like polyester blend (γ = 0.8) [19], but higher than that for the linear chain blend system (γ = 0.3) [23], suggesting that the chain structure of PMMA-POSS is somewhere between those of dendrimer-like and linear chain structures [25].

When POSS moieties are located only at the chain ends of PMMA polymers, the amount of POSS in a sample would be extremely low and the screening effect should be minimal. Therefore, in this present study we wished to investigate the effect of grafting POSS nanoparticles to the side chains of PMMA (forming so-called "PMA-POSS") on the miscibility behavior and hydrogen bonding interactions of PVPh/PMA-POSS, phenolic/PMA-POSS, and bisphenol A (BPA)/PMA-POSS blends. First, we used living anionic polymerization to prepare (Scheme 1) pure PMMA and pure PMA-POSS with similar molecular weight and narrow polydispersity indices (PDIs). We then blended PMMA and PMA-POSS individually with PVPh, phenolic resin, and BPA, with a particular interest in determining whether the POSS side chains would affect the thermal properties, miscibility behavior, and hydrogen bonding interactions of these binary blends.

2. Experimental Section

2.1. Materials

Methyl methacrylate (MMA, SHOWA, 99%) was distilled from finely ground CaH_2 prior to use. Hepta(isobutylpentacyclo-octasiloxan-1-yl)propyl methacrylate (MA-POSS, Hybrid Plastic) was dissolved in tetrahydrofuran (THF) and then precipitated into MeCN; the purified MAPOSS monomer was then recrystallized from MeOH and dried in a vacuum oven at 60 °C overnight. THF was freshly distilled over Na/benzophenone (deep purple color) after refluxing for 2 h under N_2. 1,1-Diphenylethylene (DPE) was distilled from *n*-BuLi; LiCl was dried overnight at 160 °C in a vacuum oven. *sec*-BuLi (1.3 M in cyclohexane; Chemetall) was used as obtained. Bisphenol A (molecular weight: 228.29) was supplied by the Showa Chemical (Japan). The PVPh polymer (M_w = 9000–10,000) was purchased from Polyscience (USA). The phenolic was synthesized through an H_2SO_4-catalyzed condensation reaction, producing an average molecular weight (M_n) of 500, using a procedure described previously [36–38]. Table 1 summarizes the molecular weights of all of the materials used in this study.

2.2. PMMA Homopolymer through Living Anionic Polymerization

A glass reactor containing dry LiCl (25 mg, 0.61 mmol) was charged with THF (40 mL) and then cooled to −78 °C under Ar. After 5 min, *sec*-BuLi was added until the color became light yellow. The reactor was removed from the cooling bath and warmed to room temperature until the solution becomes colorless. The reactor was again cooled to −78 °C and then 1.3 M *sec*-BuLi in cyclohexane (0.035 mL, 0.046 mmol) was added. After 5 min, DPE (0.04 mL, 0.23 mmol) was added, resulting in a deep red color. After 30 min, MMA (2 mL, 18.4 mmol) was added via cannula to the polymerization reactor with vigorous stirring. The deep red color disappeared to give a light yellow solution. After 1.5 h at −78 °C, an excess of MeOH was added to terminate the reaction. The polymer was precipitated into MeOH and dried overnight at 60 °C in a vacuum oven. Yield: 1.45 g (77%).

Table 1. Self-association and inter-association equilibrium constants and thermodynamic parameters for poly(methyl methacrylate) (PMMA) and polyhedral oligomeric silsesquioxane (PMA-POSS) and their blends with poly(vinyl phenol) (PVPh), phenolic, and bisphenol A (BPA) at 25 °C.

Polymer	V	M_w	DP	PDI	Equilibrium Constant			
					K_2	K_B	K_A [b]	K_C [c]
PVPh [a]	100	120	66	1.73	21.6	66.8	10	0
Phenolic	84	105	6	2.40	23.3	52.3	20	0
BPA	176	228	–	–	21.0	66.8	20	0
PMMA [d]	84.9	100	403	1.04	–	–	–	–
PMA-POSS [d]	826	926	41	1.07	–	–	–	–

[a] V: Molar volume (mL/mol); M_w: molecular weight of repeat unit (g/mol); DP: degree of polymerization; K_2: dimer self-association equilibrium constant; K_B: multimer self-association equilibrium constant. [b] K_A: Inter-association equilibrium constant with PMMA. [c] K_C: Inter-association equilibrium constant with PMA-POSS. [d] Molecular weights measured by multi-angle laser light scattering.

2.3. PMA-POSS Homopolymer through Living Anionic Polymerization

A glass reactor containing dry LiCl (13 mg, 0.31 mmol) was charged with THF (40 mL) and then cooled to −78 °C under Ar. After 5 min, *sec*-BuLi was added until the color became light yellow. The reactor was removed from the cooling bath and warmed to room temperature until the solution becomes colorless. The reactor was again cooled to −78 °C and then 1.3 M *sec*-BuLi in cyclohexane (0.018 mL, 0.023 mmol) was added. After 5 min, DPE (0.021 mL, 0.12 mmol) was added, resulting in a deep red color. After 30 min, a solution of MA-POSS (2.00 g, 2.1 mmol) in THF (6.0 mL) was added from to the polymerization reactor via cannula with vigorous stirring. The deep red color disappeared to give a colorless solution. After 9 h at −78 °C, an excess of MeOH was added to terminate the reaction. The polymer was then precipitated into MeOH and dried overnight at 60 °C in a vacuum oven. Yield: 1.55 g (78%).

2.4. Blend Preparations

Blends of phenolic/PMMA, PVPh/PMMA, BPA/PMMA, phenolic/PMA-POSS, PVPh/PMA-POSS, and BPA/PMA-POSS at various compositions were prepared through solution-casting. A THF solution containing 5 wt% of the polymer mixture was stirred for 6–8 h and then the solvent was evaporated slowly at 50 °C for 1 day. The film of the blend was then dried at 80 °C for 2 days to ensure total removal of residual solvent.

2.5. Characterization

^{1}H, ^{13}C, and ^{29}Si NMR spectra were recorded at room temperature using a Bruker AM 500 (500 MHz) spectrometer, with the residual proton resonance of the deuterated solvent as the internal standard. Molecular weights and molecular weight distributions were determined through gel permeation chromatography (GPC) using a Waters 510 high-performance liquid chromatograph equipped with a 410 differential refractometer and three Ultrastyragel columns (100, 500, and 10^3 Å) connected in series, with THF as the eluent (flow rate: 1.0 mL/min). DSC was performed using a TA-Q20

instrument operated at a scan rate of 20 °C/min over a temperature range from 0 to 250 °C under a N_2 atmosphere. FTIR spectra of the polymer films, sufficiently thin to obey the Beer–Lambert law, were recorded using the conventional KBr disk method and a Bruker Tensor 27 FTIR spectrophotometer; 32 scans were collected at a spectral resolution of 1 cm^{-1}. As polymers containing OH groups are hygroscopic, pure N_2 gas was used to purge the spectrometer's optical box to ensure dry sample films. FTIR spectra of samples at elevated temperatures were recorded using a cell mounted within the temperature-controlled compartment of the spectrometer. WAXD data were collected using the BL17A1 wiggler beamline of the National Synchrotron Radiation Research Center (NSRRC), Taiwan. A triangular bent Si (111) single crystal was employed to obtain a monochromated beam having a wavelength (λ) of 1.33001 Å.

3. Results and Discussion

3.1. Synthesis of PMA-POSS

Hirai *et al.* have reported that PMA-POSS homopolymers can be prepared through living anionic polymerization when using *sec*-BuLi as the initiator in the presence of excess LiCl and 1,1-diphenylethylene (DPE) at −78 °C [39]. In this study, we used a similar method to prepare the PMA-POSS homopolymer. Figure 1 displays the ^{1}H, ^{13}C, and ^{29}Si NMR spectra and MALS analysis data of our pure PMA-POSS homopolymer. The ^{1}H NMR spectrum (Figure 1a) of PMA-POSS features the signal for the $SiCH_2$ (a) unit of the POSS cage at 0.59 ppm and for the OCH_2 (g) unit of the side chain at 3.76 ppm; the ^{13}C NMR spectrum (Figure 1b) features the signals of their carbon nuclei at 23.05 and 69.78 ppm, respectively. The ^{29}Si NMR spectrum (Figure 1c) possesses two sharp signals at −68.4 and −68.0 ppm corresponding to the silicon nuclei of the POSS units. The GPC analysis in Figure 1d suggests a number-average molecular weight (M_n) for the PMA-POSS sample prepared in this study of 38,300 g/mol and a PDI of 1.07. Taken together, the ^{1}H, ^{13}C, and ^{29}Si NMR spectra and the GPC analysis confirmed the successful synthesis of PMA-POSS.

3.2. DSC Analyses

Figure 2a,b displays conventional second-run DSC thermograms of PMMA and PMA-POSS, respectively, in the presence of PVPh at various weight ratios. In this study, the glass transition temperatures of PMMA and PMA-POSS were 131 and 59 °C, respectively. This value of T_g for PMA-POSS was close to that reported previously after living anionic polymerization [39]. The value of T_g of poly(*n*-propyl methacrylate) (PPMA) has been reported to be approximately 35 °C; therefore, the increase in the glass transition temperature for PMA-POSS (to 59 °C) was presumably due to the nano-reinforcement effect of the rigid cubic silsesquioxane core of the POSS units on the PPMA segments, effectively restricting their molecular chain motion [40–42]. Figure 2a presents the second heating runs in our DSC analyses of PVPh/PMMA blends at various compositions; all blend compositions exhibited a single glass transition temperature over the entire range of compositions, indicating that they were fully miscible and featured a homogeneous amorphous phase. In contrast, the DSC thermograms of the PVPh/PMA-POSS blend (Figure 2b) displays two values of T_g, implying that the components were phase-separated in the amorphous phase. The value of T_g of the PMA-POSS

domain decreased slightly upon increasing the PVPh content; in contrast, the value of T_g of the PVPh domain increased upon increasing the PMA-POSS content.

Figure 1. Characterization of PMA-POSS homopolymer: (**a**) ^{1}H; (**b**) ^{13}C; and (**c**) ^{29}Si NMR spectra; and (**d**) MALS analysis.

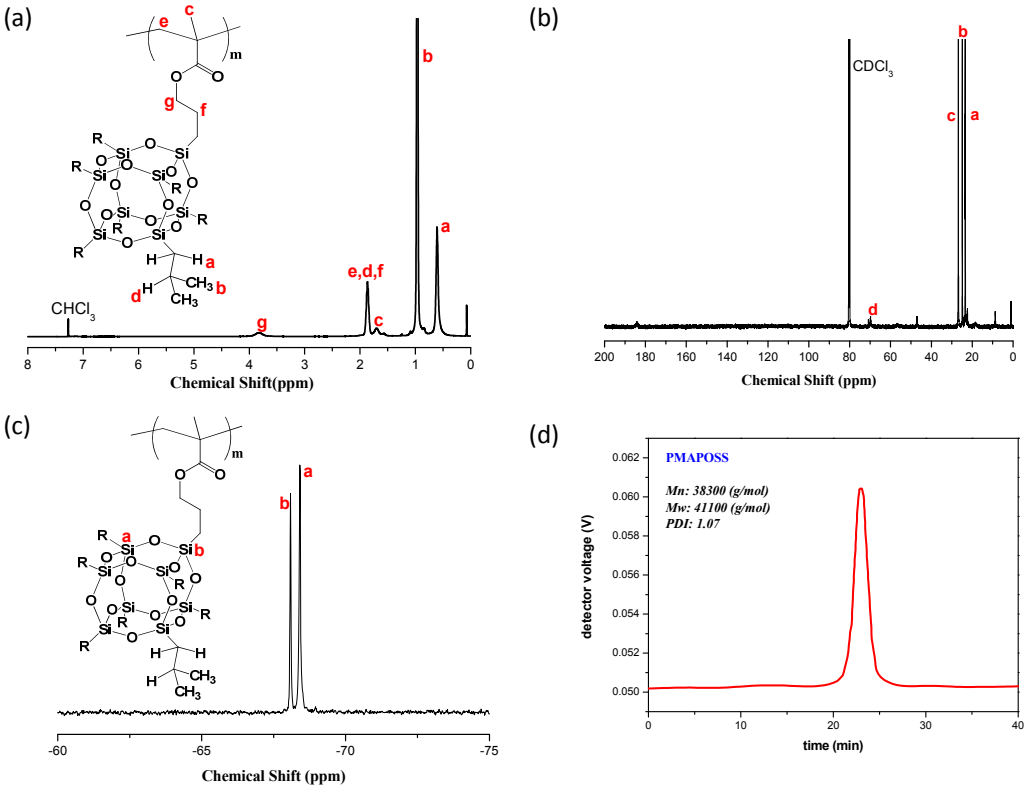

Figure 2. DSC thermograms of (**a**) PMMA and (**b**) PMA-POSS blends containing various PVPh compositions (weight ratio).

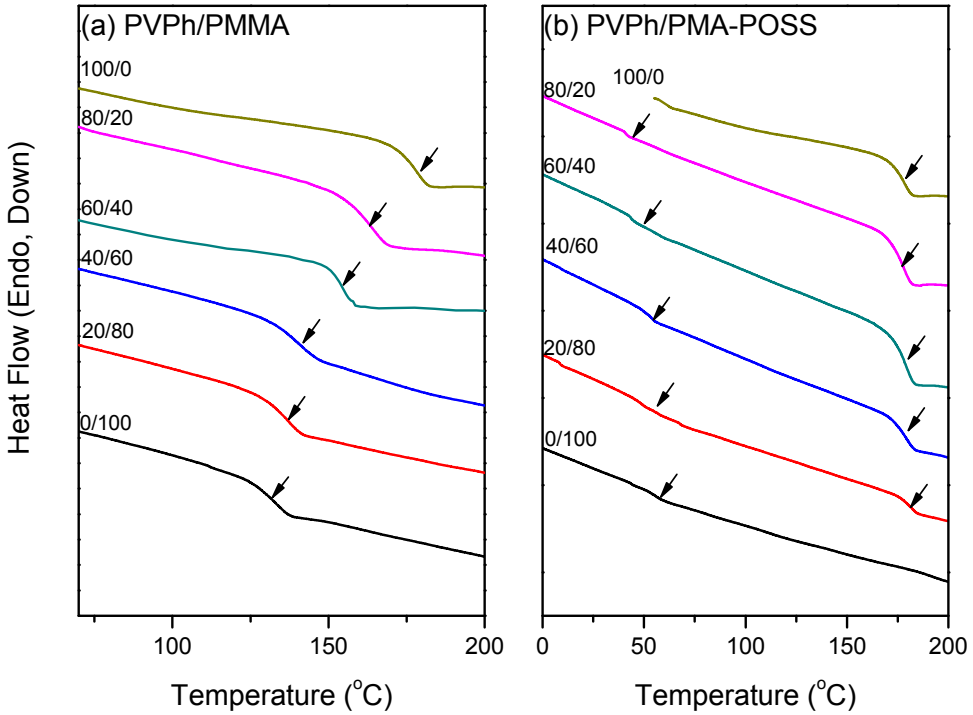

Figure 3a,b presents the conventional second-run DSC thermograms of PMMA and PMA-POSS, respectively, with phenolic blends at various weight ratios. Similar to the results for PVPh/PMMA and PVPh/PMA-POSS, the phenolic/PMMA blend compositions exhibited a single glass transition temperature, implying miscible blends; in contrast, the phenolic/PMA-POSS blends provided two values of T_g, implying phase-separation in the amorphous phase. The value of T_g of the PMA-POSS domain also decreased slightly upon increasing the phenolic content, whereas the value of T_g of the phenolic domain increased upon increasing the PMA-POSS content. Figure 4a,b summarizes the glass transition temperatures for the PVPh/PMA-POSS and phenolic/PMA-POSS blends, respectively.

Figure 3. DSC thermograms of (**a**) PMMA and (**b**) PMA-POSS blends containing various phenolic compositions (weight ratio).

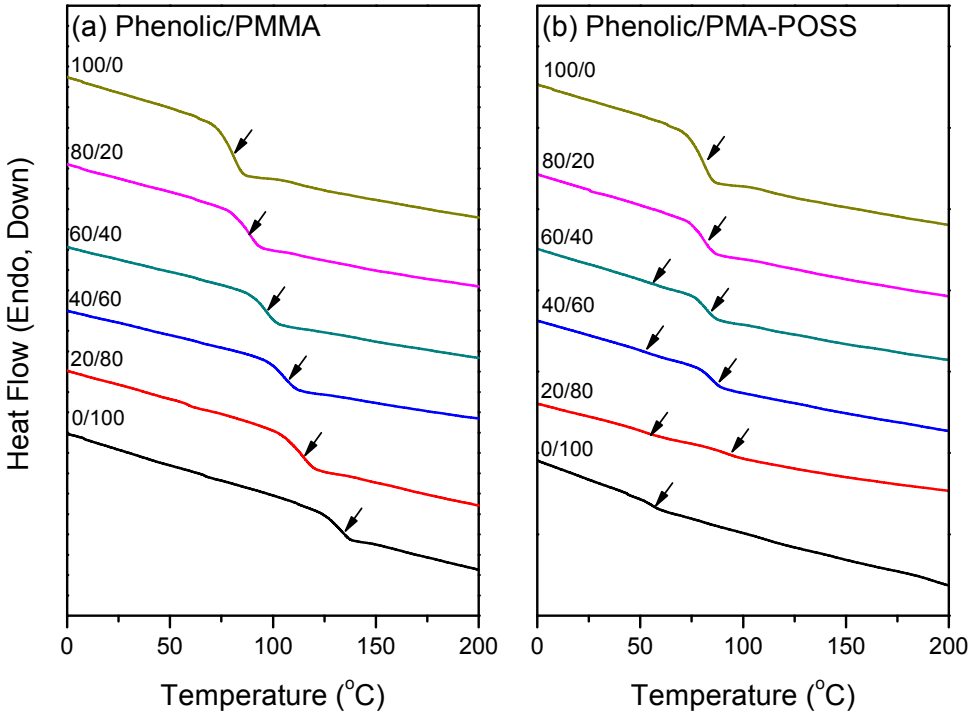

Next, we investigated the blending of bisphenol A (BPA)—a crystalline, low-molecular-weight, hydrogen bond donor compound—with PMMA and PMA-POSS. Although the molar mass of BPA is only 228, it features a single glass transition temperature at 42.5 °C during its second heating scan; pure BPA also possesses a melting temperature of 162.3 °C [43]. The binary blends of BPA/PMMA were totally miscible in the amorphous phase, as evidenced by a single glass transition temperature in the DSC analyses in Figure 5a. In addition, the signal for the melting temperature of the BPA component disappeared upon increasing the PMMA content. In contrast, the melting temperatures for the BPA/PMA-POSS blends decreased slightly upon increasing the PMA-POSS content, but plateaued at relatively high PMA-POSS contents, indicating that BPA did not dissolve completely in PMA-POSS (phase-separated blends). As the values of T_g of BPA and PMA-POSS were similar, it was difficult to discern the miscibility behavior based on DSC analysis. We could, however, conclude that the intermolecular interactions in the BPA/PMMA and BPA/PMA-POSS blends were quite different because of the distinct crystallization behavior of the BPA phases within them.

Figure 4. Glass transition temperature–composition curves of (**a**) PVPh/PMA-POSS and (**b**) phenolic/PMA-POSS blends.

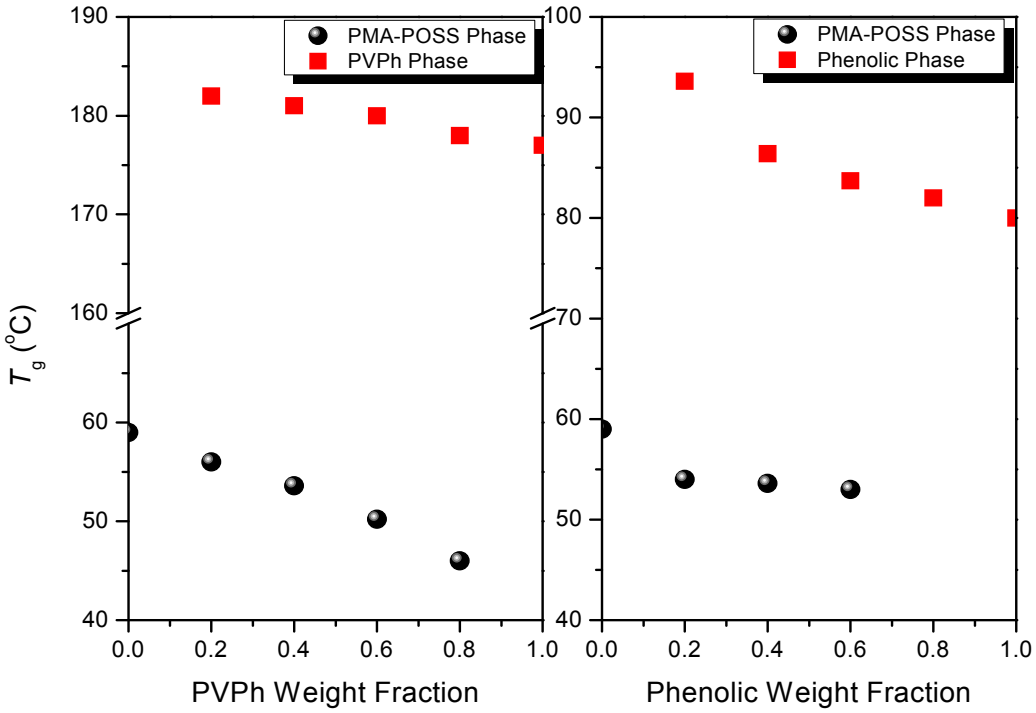

Figure 5. DSC thermograms of (**a**) PMMA and (**b**) PMA-POSS blends containing various BPA compositions (weight ratio).

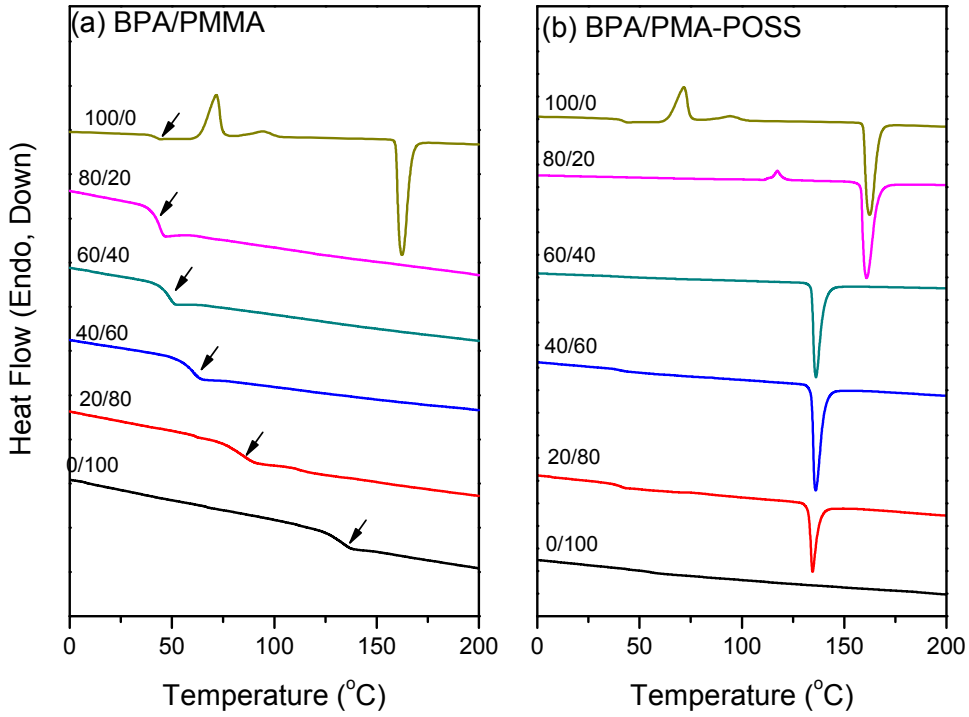

Figure 6 summarizes the behavior of the glass transition temperatures of PVPh/PMMA, phenolic/PMMA, and BPA/PMMA. All of these blends featured a composition-dependent single value

of T_g, indicating that they were all fully miscible. In general, the relationship between the glass transition temperature and the composition of a miscible polymer blend follows the Kwei equation [44]:

$$T_g = \frac{W_1 T_{g1} + kW_2 T_{g2}}{W_1 + kW_2} + qW_1 W_2 \quad (1)$$

where W_1 and W_2 are the weight fractions of the components, T_{g1} and T_{g2} represent the corresponding glass transition temperatures, and k and q are fitting constants. The parameter q corresponds to the strength of specific interactions in the blend, reflecting a balance between the breaking of self-association interactions and the formation of inter-association interactions. As displayed in Figure 6, using a non-linear least-squares "best fit" approach we obtained values of k and q for the PVPh/PMMA blends of 1 and −20, respectively; for the phenolic/PMMA blends of 1 and −15, respectively; and for the BPA/PMMA blends of 1 and −120, respectively. The negative values of q indicate that the inter-association equilibrium constants (or average hydrogen bonding strengths) for the OH···C=O interactions were less than the self-association equilibrium constants for the OH···OH interactions in these three binary blends. Here, we compare only the results for PVPh/PMMA and phenolic/PMMA, because BPA is a low-molecular-weight compound having a crystal structure that is different from those of PVPh and phenolic resin. We conclude from this study that the average hydrogen bonding strength of phenolic/PMMA was larger than that of PVPh/PMMA, consistent with our previous finding that phenolic is a more acidic hydrogen bond donor polymer relative to PVPh [45].

Figure 6. Glass transition temperature–composition curves, based on the Kwei equation, of PVPh/PMMA, phenolic/PMMA, and BPA/PMMA blends.

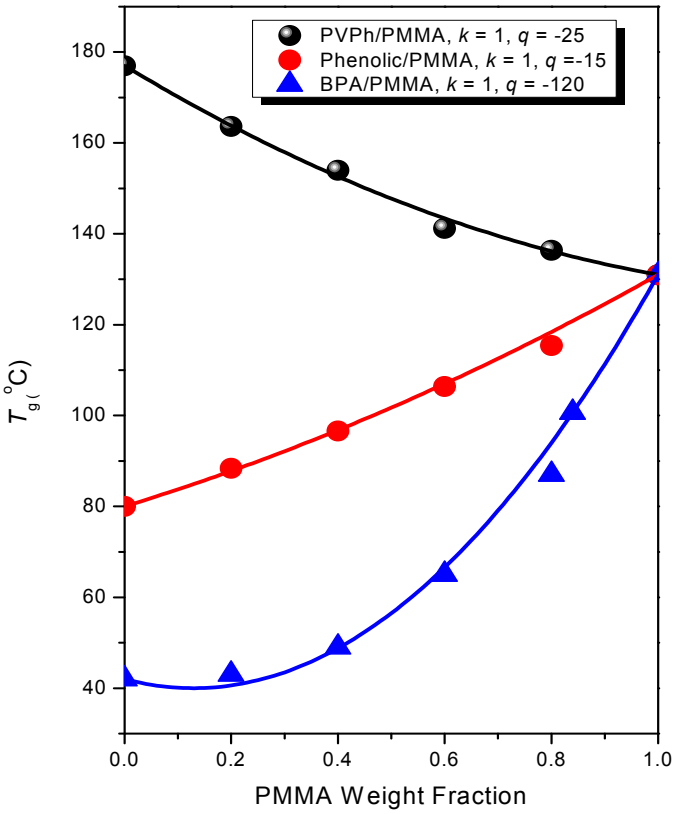

3.3. FTIR Spectra of PMMA Homopolymer Blend Systems

Infrared (IR) spectroscopy can provide positive information regarding the specific interaction between polymers, both qualitatively and quantitatively. The OH stretching range in an IR spectrum is sensitive to the presence of hydrogen bonds. Figure 7 presents the OH stretching regions of the FTIR spectra of PVPh/PMMA, phenolic/PMMA, and BPA/PMMA blends recorded at room temperature. The spectra of pure PVPh, phenolic, and BPA feature two distinct bands in the OH-stretching region of the FTIR spectra: a very broad band centered at 3350, 3360, and 3330 cm^{-1}, respectively, representing the wide distribution of the hydrogen bonded OH groups and a sharp band near 3525 cm^{-1}, caused by the free OH groups. In general, the intensity of the signal for the free OH groups decreased upon increasing the PMMA content, as would be expected. Meanwhile, the broad signal for the hydrogen-bonded OH groups shifted to higher frequency—to 3450, 3430, and 3445 cm^{-1} for phenolic, PVPh, and BPA, respectively—upon increasing the PMMA content to 80 wt%. All these observed changes arose from transformations from strong intramolecular OH···OH bonds to weak intermolecular OH···C=O bonds.

Figure 7. FTIR spectra (4000–2700 cm^{-1} region) recorded at room temperature for (**a**) PVPh/PMMA; (**b**) phenolic/PMMA; and (**c**) BPA/PMMA blends containing various PMMA compositions.

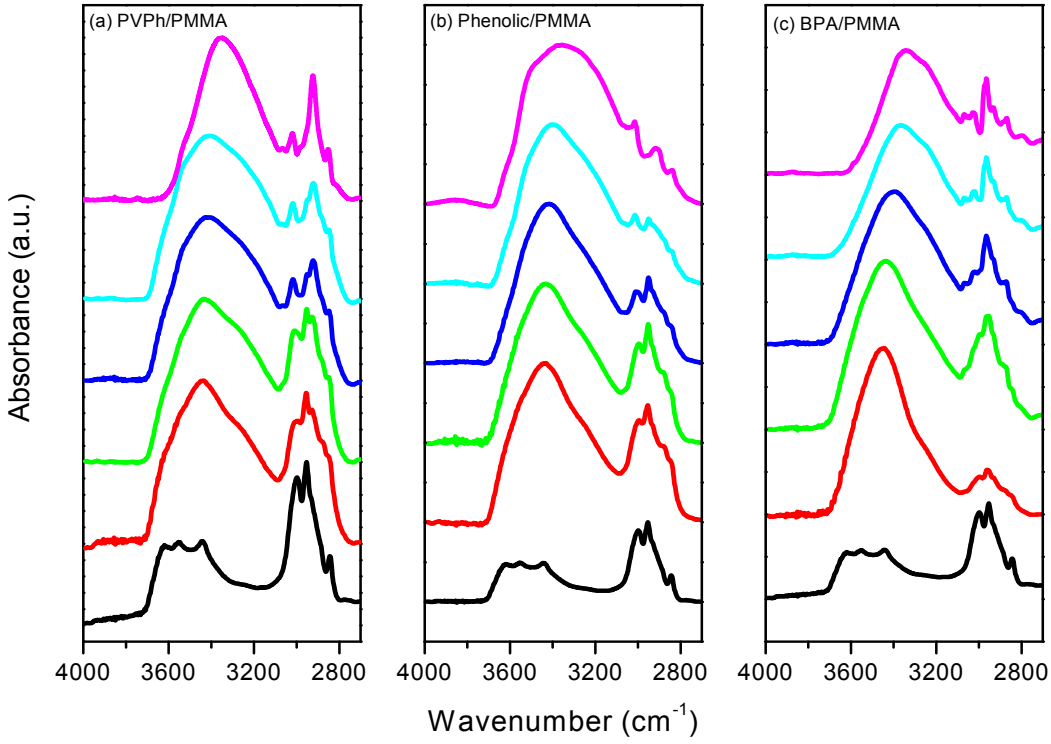

These results are consistent with the negative values of q obtained using the Kwei equation. Coleman *et al.* [1] have suggested using the frequency difference (Δv) between the signals for the hydrogen-bonded and free OH units as a measure of the average strength of the intermolecular interactions. In this study, we found that the average strength of the hydrogen bonds between the C=O

groups of PMMA and the OH groups of the three OH-containing compounds followed the order phenolic/PMMA ($\Delta\nu$ = 95 cm^{-1}) > BPA/PMMA ($\Delta\nu$ = 80 cm^{-1}) > PVPh/PMMA ($\Delta\nu$ = 75 cm^{-1}).

In addition to the OH stretching region, the C=O stretching was also sensitive to hydrogen bond formation. Figure 8 displays the C=O stretching region of the FTIR spectra of PVPh/PMMA, phenolic/PMMA, and BPA/PMMA recorded at room temperature. All of the C=O stretching frequencies were split into two bands, which could be fitted well to the Gaussian function, as displayed in Figure 9. One band, with absorption at 1730 cm^{-1}, corresponds to the free C=O groups; the other, located at 1708, 1706, and 1706 cm^{-1} for phenolic, PVPh, and BPA, respectively, represents the hydrogen-bonded C=O groups. The fraction of hydrogen-bonded C=O groups can be calculated using an appropriate absorptivity ratio ($a_R = a_{HB}/a_F$ = 1.5), as has been discussed previously [1]. Table 2 summarizes the results from curve fitting; Figure 10 displays the fraction of hydrogen-bonded C=O groups in the individual binary polymer blends of PVPh/PMMA, phenolic/PMMA, and BPA/PMMA.

On the basis of the Painter–Coleman association model, we determined the inter-association equilibrium constants for PVPh/PMMA, phenolic/PMMA, and BPA/PMMA, using a least-squares method, as has been described previously [46]. Table 1 lists all of the thermodynamic parameters in these three polymer blend systems. K_2 and K_B represent the self-association equilibrium constants for hydrogen-bonded dimers and multimers, respectively, of PVPh, phenolic, and BPA; K_A represents the equilibrium constant describing the inter-association of PMMA with PVPh, phenolic, or BPA. We determined the inter-association equilibrium constants (K_A) for the PVPh/PMMA, phenolic/PMMA, and BPA/PMMA blends to be approximately 10, 20, and 20, respectively, as shown in Figure 10.

Figure 8. FTIR spectra (1800–1650 cm^{-1} region) recorded at room temperature for (**a**) PVPh/PMMA; (**b**) phenolic/PMMA; and (**c**) BPA/PMMA blends containing various PMMA compositions.

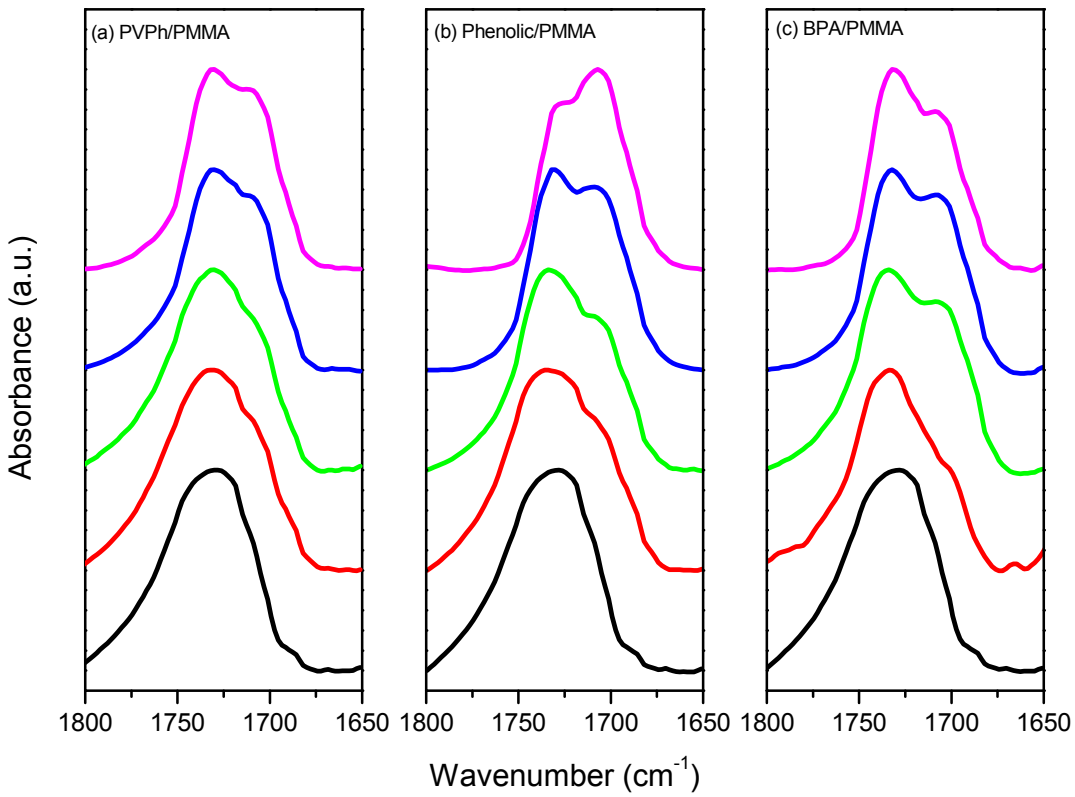

Figure 9. Deconstructed models of the C=O stretching bands (in Figure 8) with respect to the weight percentages of (**a**) PVPh/PMMA, (**b**) phenolic/PMMA, and (**c**) BPA/PMMA blends at various compositions.

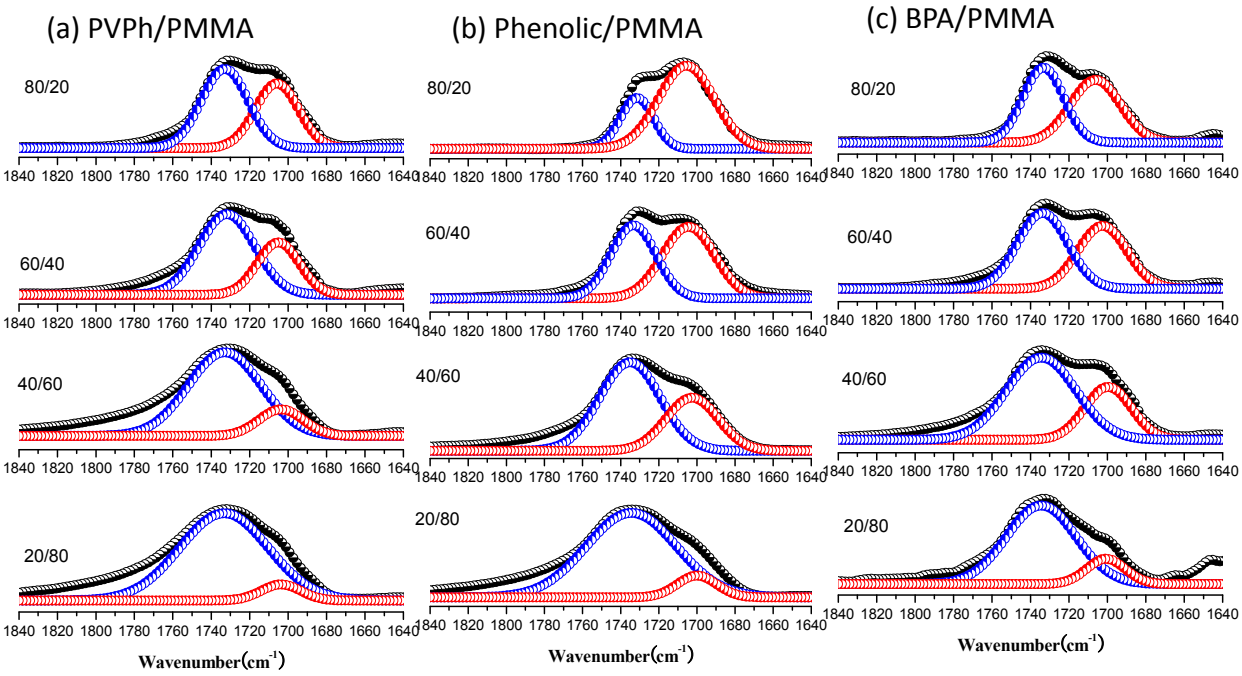

Table 2. Curve-fitting of the Fourier transform infrared (FTIR) spectroscopic data for the C=O groups of PMMA and its blends with PVPh, phenolic, and BPA.

Sample (wt%)	Free C=O		Hydrogen-bonded C=O		f_b (%)
	ν_f (cm^{-1})	A_f (%)	ν_b (cm^{-1})	A_b (%)	
PVPh/PMMA					
0/100	1734	100	–	–	–
20/80	1733	92.4	1704	7.6	5.1
40/60	1733	83.9	1704	16.1	11.3
60/40	1732	67.2	1705	32.8	24.5
80/20	1733	57.0	1705	43.0	33.4
Phenolic/PMMA					
20/80	1734	84.9	1703	15.1	10.6
40/60	1735	65.9	1703	34.1	25.6
60/40	1733	46.8	1704	53.2	43.1
80/20	1732	26.8	1705	73.2	64.5
BPA/PMMA					
20/80	1734	89.9	1705	10.1	6.9
40/60	1734	69.8	1705	30.2	22.3
60/40	1734	55.2	1705	44.8	35.1
80/20	1733	49.2	1705	50.8	40.7

ν_f: Wavenumber of signal for free C=O groups of PMMA; ν_b: wavenumber of signal for hydrogen-bonded C=O groups of PMMA; A_f: area fraction of signal for free C=O groups of PMMA; A_b: area fraction of hydrogen-bonded C=O groups of PMMA; f_b: fraction of hydrogen-bonded PMMA = $(A_b/1.5)/(A_b/1.5 + A_f)$.

Figure 10. Fraction of hydrogen-bonded C=O groups of PMMA in the presence of different hydrogen bonding donor compounds, determined from FTIR spectra, and values of K_A calculated using the Painter–Coleman association model.

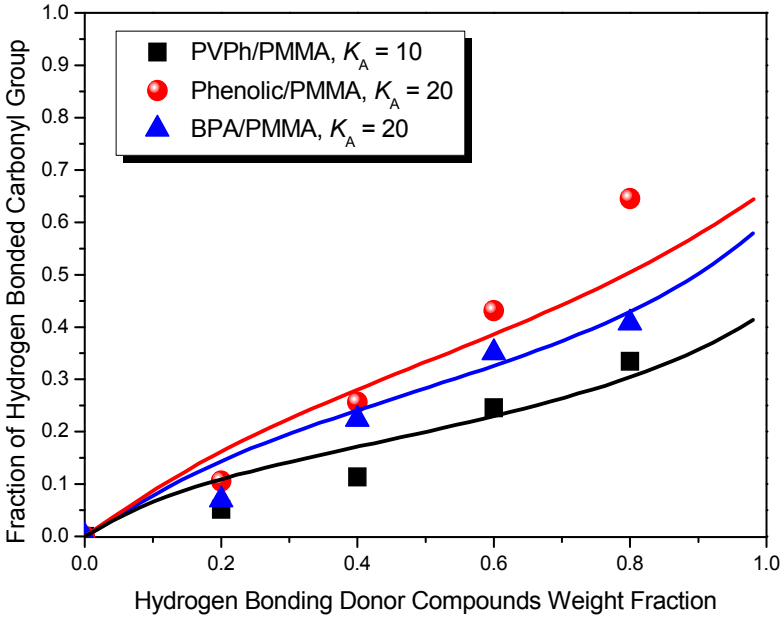

The value of K_A for the phenolic/PMMA blend is similar to that we had determined in a previous study [25]; in contrast, the value of K_A for the PVPh/PMMA blend is smaller than those found in previous studies [11], presumably because of the different solvents employed in the different blend preparations. The implication here is that miscibility may be achieved when THF is used to cast the blend, but not when methyl isobutyl ketone (MIBK) is used as the solvent, as in the previous studies [11]. This phenomenon can be explained by considering the compositional heterogeneities that arise from the different solvent molecules, as has been discussed widely in previous studies [6–9,22]. Dong *et al.* [9] indicate that in solvent-cast PVPh + PMMA limited hydrogen-bonding interaction exists when THF is used, due to the strong hydrogen-bonding affinity of THF that develops hydrogen bonds with the polymer molecules, compared to the weaker hydrogen-bonding affinity of MIBK. Here, we choose THF as our cast solvent because PMA-POSS was not soluble in MIBK. For comparison with the PMA-POSS blend system, we also choose to study the PMMA blend system in THF solution. Clearly, the inter-association equilibrium constants and relative ratios of K_A/K_B followed the order phenolic/PMMA > BPA/PMMA > PVPh/PMMA. In these three binary blends, however, the OH groups of PVPh, phenolic, and BPA could still interact readily with the C=O groups of PMMA, even though their donor abilities were different.

3.4. FTIR Spectra of PMMA-POSS Homopolymer Blend Systems

Figure 11 displays the C=O stretching regions of the FTIR spectra of PVPh/PMA-POSS, phenolic/PMA-POSS, and BPA/PMA-POSS recorded at room temperature. The blending of the PMA-POSS homopolymer with these hydrogen bond donor compounds was clearly quite different from that of the PMMA homopolymer. We did not observe any hydrogen-bonded C=O groups of PMA-POSS when blending with the polymer PVPh or phenolic or even with the low-molecular-weight

compound BPA. We rationalize this phenomenon in terms of the so-called "screening effect." The value of the intramolecular screening parameter (γ) for a linear chain structure blend (e.g., PVPh/PMMA) is approximately 0.3, whereas that of a dendrimer-like polyester blend (e.g., PVPh/dendrimer-like polyester) is approximately 0.8 [19,23]. From a previous study [25], we reported that a value of γ of 0.65 for a phenolic/PMMA-POSS block copolymer blend in which the POSS nanoparticles were positioned at the chain end of the PMMA polymer. In this present study, the values of γ were all very close to 1 for the PVPh/PMA-POSS, phenolic/PMA-POSS, and BPA/PMA-POSS blend systems, in which the POSS nanoparticles were located on the side chains of the PMMA polymer. As a result, the C=O groups of PMA-POSS could not interact through intermolecular hydrogen bonding with the OH groups of the hydrogen bond donor compounds. This behavior presumably arose for two main reasons: (i) the inter-association equilibrium constant between the OH groups and the POSS units (K_A = 38.6) [47,48] being greater than that between the OH and C=O groups (K_A = 20) [25]; (ii) strong aggregation of the POSS nanoparticles on the PMMA side chains. We also tested the effect of increased temperature on the hydrogen bonding interactions in the phenolic/PMA-POSS blend (Figure 12). Again, we did not observe any C=O groups hydrogen bonded with the phenolic resin: only the signal for the self-association of the OH···OH groups shifted to higher wavenumber when we disrupted the strong aggregation of the POSS nanoparticles upon increasing the temperature.

Figure 11. FTIR spectra (1800–1650 cm^{-1} region) recorded at room temperature for (**a**) PVPh/PMA-POSS; (**b**) phenolic/PMA-POSS; and (**c**) BPA/PMA-POSS blends containing various PMMA compositions.

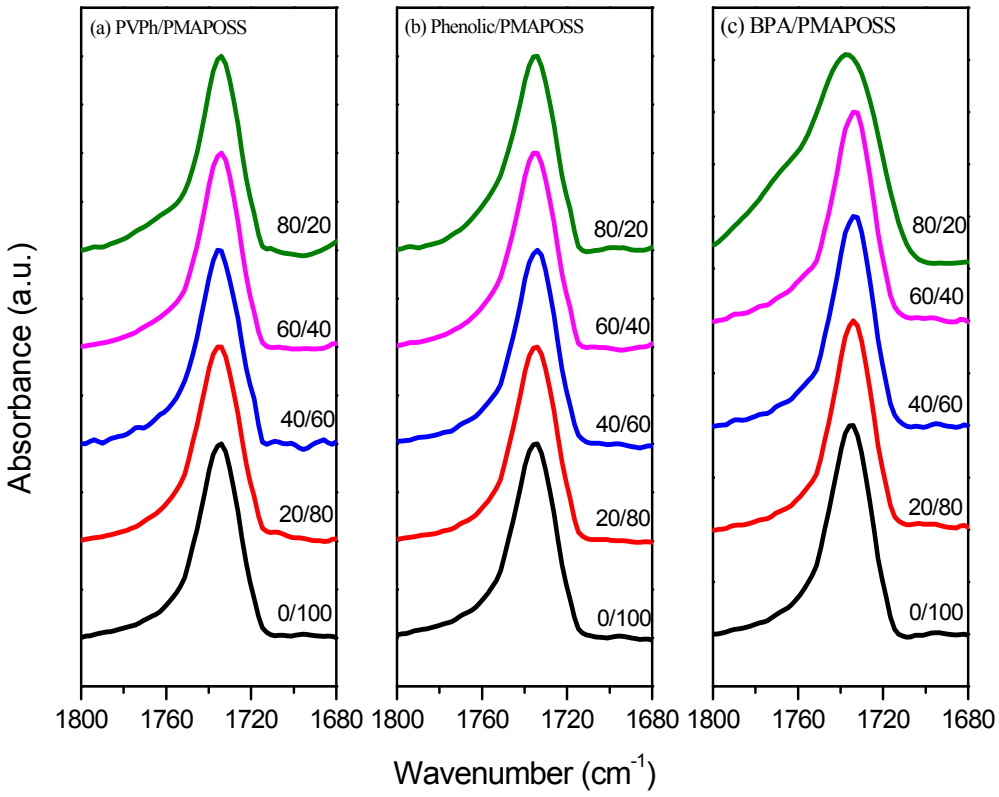

Figure 12. FTIR spectra of phenolic/PMA-POSS = 60/40, recorded at various temperatures: (**a**) OH stretching and (**b**) C=O stretching regions.

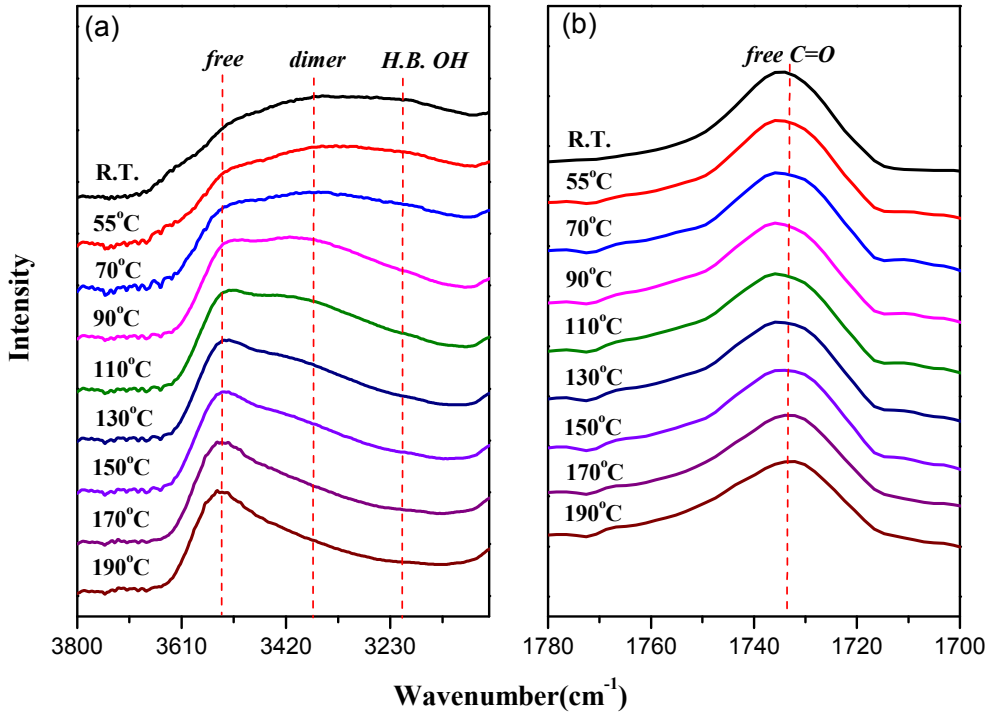

3.5. WAXD Analyses of PMMA-POSS Homopolymer Blend Systems

Figure 13 presents X-ray diffraction patterns of the phenolic/PMA-POSS, BPA/PMA-POSS, and BPA/PMMA blends at room temperature. Here, we did not investigate the PVPh/PMA-POSS blends because their X-ray diffraction patterns were similar to those of phenolic/PMA-POSS blends. Pure PMA-POSS provided two major diffraction peaks at values of 2θ of 7.50 and 15.99°, corresponding to *d*-spacings of 1.0 and 0.49 nm, respectively [39,49]; the first is consistent with the size of a POSS unit and was produced by the rhombohedral crystal structure of the POSS units [50], where a *d*-spacing of 0.49 nm is the average distance between the $COOCH_2$ groups of the PMA-POSS segments [39]. No X-ray diffraction peaks were discernible for the pure phenolic resin; only an amorphous halo appeared at a value of 2θ of 16.23° in Figure 13a. In contrast, many strong diffraction peaks are evident in Figure 13b,c, indicating highly crystalline structures for pure BPA [51]. Clear signals at a value of 2θ of 7.50° were also present in the diffraction patterns of the phenolic/PMA-POSS and BPA/PMA-POSS blends, indicating that POSS crystals with one dimension approximately equal to 1 nm remained in these blend systems.

In Figure 13b, peaks for crystalline BPA appear in the X-ray diffraction pattern of the BPA/PMA-POSS blend, indicating that the BPA molecules could not dissolve completely in PMA-POSS (phase-separated blends). The results are quite different for the BPA/PMMA blends; the crystallinity of BPA decreased upon increasing of PMMA content (Figure 13c). These WAXD data for BPA blends with PMMA and PMA-POSS are consistent with our DSC data in Figure 5, where the signal for the melting temperature of the BPA component disappeared upon increasing the PMMA content. In contrast, the melting temperatures for the BPA/PMA-POSS blends decreased slightly upon increasing the PMA-POSS content, but plateaued at relatively high PMA-POSS contents. In general,

the crystallinity measured using WAXD is an *in situ* measurement with no thermal history involved in preparing the sample. In contrast, the crystallinity detected by DSC depends on the thermal history; accordingly, we did not observe melting peaks for the BPA/PMMA blends through DSC analyses [52].

Figure 13. WAXD patterns of (**a**) phenolic/PMA-POSS; (**b**) BPA/PMA-POSS; and (**c**) BPA/PMMA blends, recorded at room temperature.

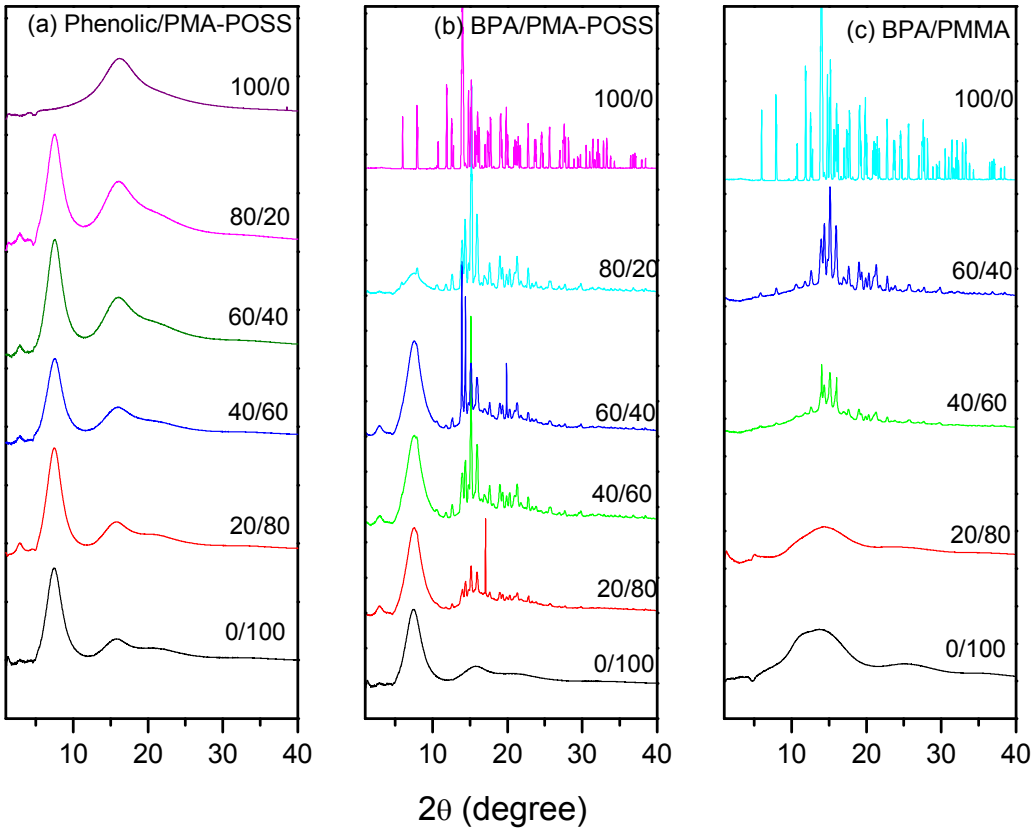

We also observed a weak diffraction peak at a value of 2θ of 3.0°, corresponding to a *d*-spacing of 2.6 nm, in the X-ray diffraction patterns of both the phenolic/PMA-POSS and BPA/PMA-POSS blends; we attribute this signal to the average distance between the main chains of PMA-POSS [39]. Jin *et al.* reported that PMA-POSS chains are randomly oriented, without any ordering, in solvent-annealed films, whereas thermally-annealed PMA-POSS forms regularly packed molecular cylinders in a helical conformation in an orthorhombic lattice unit cell as a result of crystallization of the POSS moieties; through simulation, they estimated the size of the PMA-POSS chains in the helical conformation to be approximately 2.5 nm [39]. As a result, the strong aggregation through crystallization of the POSS nanoparticles was also enhanced after blending with phenolic resin or BPA, implying that the OH groups of the phenolic or BPA did not have the opportunity to interact with the C=O groups of PMA-POSS (Scheme 2) and, thus, these binary blends appeared as immiscible blend systems during DSC analyses, due to both strong screening effects and the aggregation ability of the POSS nanoparticles.

Scheme 2. Schematic illustration of relevant length scale in PMA-POSS, and possible phase structure of phenolic/PMA-POSS blend, where PMA-POSS assume a helix-like structure.

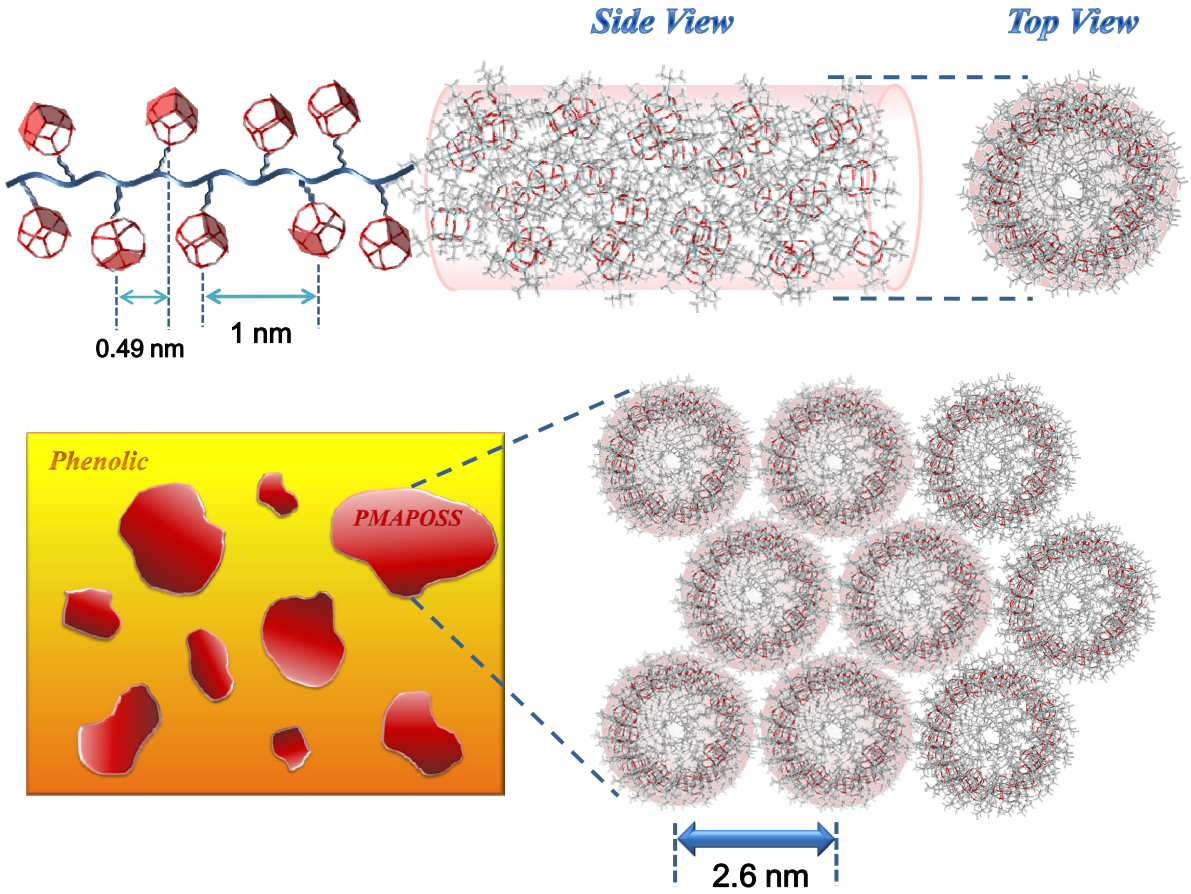

We also investigated the WAXD patterns of phenolic/PMA-POSS and BPA/PMA-POSS at various temperatures (Figure 14). The intensity of the diffraction peak at a value of 2θ of 3.0° increased upon increasing the temperature, indicating that thermal annealing of the PMA-POSS main chains did indeed enhance the regularly packing as molecular cylinders in a helical conformation in an orthorhombic lattice unit cell. In addition, the crystal peak from BPA disappeared (Figure 14b) when the temperature (180 °C) was above the melting temperature of BPA (162 °C), consistent with DSC analyses in Figure 5b. From the FTIR spectra in Figure 12, we observe that only the signal for the OH···OH self-association shifted to higher wavenumber—the signal for the free C=O groups of PMA-POSS did not change—upon increasing the temperature, again indicating that this phenolic/PMA-POSS blend was an immiscible system in which the OH groups of phenolic did not have the ability to interact with the C=O groups of PMA-POSS. Here, we proposed that the values of γ should be very close to 1 for all of the PVPh/PMA-POSS, phenolic/PMA-POSS, and BPA/PMA-POSS blend systems when the POSS nanoparticles were present on the side chains of PMMA, because strong aggregation of the POSS units induced a strong "screening effect" for the C=O groups of PMA-POSS.

Figure 14. WAXD patterns of (**a**) phenolic/PMA-POSS = 60/40 and (**b**) BPA/PMA-POSS = 60/40 blends, recorded at various temperatures

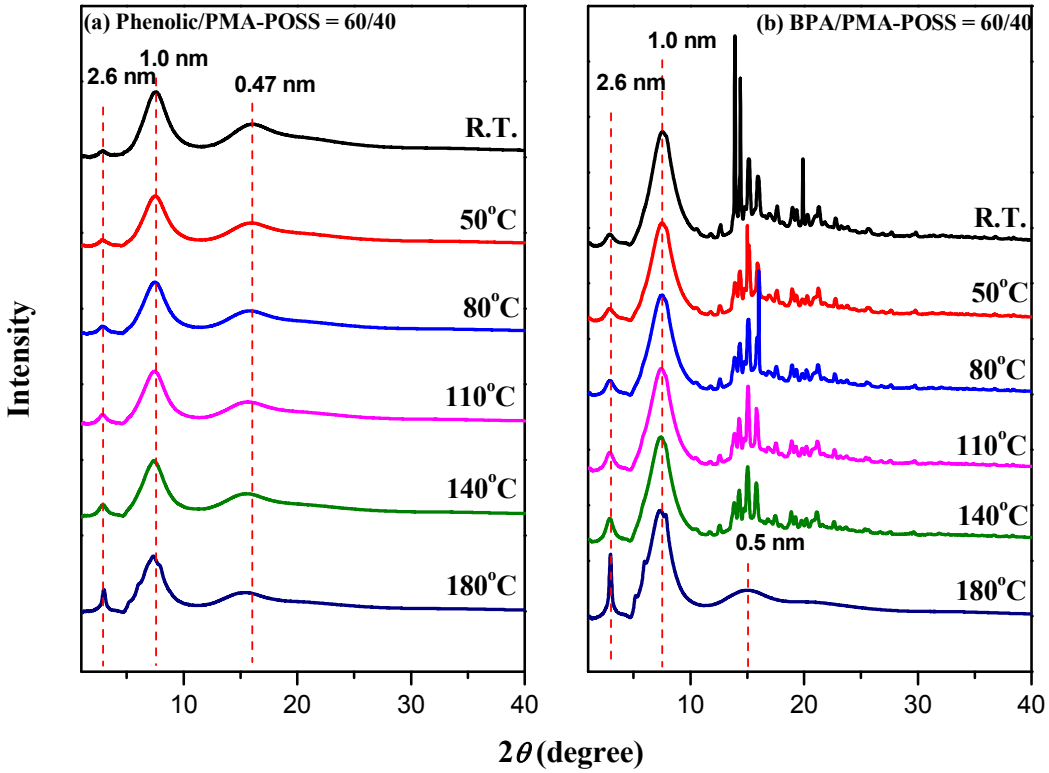

4. Conclusions

We have prepared a series of blends of PMMA and PMA-POSS with PVPh, phenolic resin, and BPA and investigated their properties using DSC, FTIR spectroscopy, and WAXD. All of these blends of PMMA with PVPh, phenolic, and BPA were totally miscible in the amorphous phase over their entire compositions, as evidenced by a single glass transition temperature (DSC) and intermolecular hydrogen bonding interactions (FTIR spectroscopy) between the C=O groups of PMMA and the OH groups of PVPh, phenolic, and BPA. FTIR spectra revealed the absence of hydrogen bonding interactions between the C=O groups of PMA-POSS (with POSS units present on the side chains) and the OH groups of PVPh, phenolic, and BPA. The strong "screening effect" in these blends induced by the tethered POSS side chains induced immiscibility with the hydrogen bond donor compounds. The strong aggregation, through crystallization, of the POSS nanoparticles (observed in WAXD analyses) was enhanced after blending with phenolic resin or BPA compounds, implying that the OH groups of PVPh, phenolic, and BPA could not interact with the C=O groups of PMA-POSS; accordingly, DSC analyses indicated that these binary blends were immiscible systems.

Acknowledgments

This study was supported financially by the National Science Council, Taiwan, under contracts NSC 100-2221-E-110-029-MY3 and NSC 102-2221-E-110-008-MY3. Lin thanks the Interchange Association of Japan for their summer visit program, which helped initiate this study.

Conflicts of Interest

The authors declare no conflict of interest.

References

1. Coleman, M.M.; Painter, P.C. Hydrogen bonded polymer blends. *Prog. Polym. Sci.* **1995**, *20*, 1–59.
2. He, Y.; Zhu, B.; Inoue, Y. Hydrogen bonds in polymer blends. *Prog. Polym. Sci.* **2004**, *29*, 1021–1051.
3. Kuo, S.W. Hydrogen-bonding in polymer blends. *J. Polym. Res.* **2008**, *15*, 459–486.
4. Kuo, S.W.; Huang, C.F.; Tung, P.H.; Huang, W.J.; Huang, J.M.; Chang, F.C. Synthesis, thermal properties, and specific interactions of high T_g increase in poly(2,6-dimethyl-1,4-phenylene oxide)-*block*-polystyrene copolymers. *Polymer* **2005**, *46*, 9348–9361.
5. Kuo, S.W.; Huang, W.J.; Huang, C.F.; Chan, S.C.; Chang, F.C. Miscibility, Specific Interactions, and Spherulite Growth Rates of Binary Poly(acetoxystyrene)/Poly(ethylene oxide) Blends. *Macromolecules* **2004**, *37*, 4164–4173.
6. Zhang, X.; Takegoshi, K.; Hikichi, K. Poly(vinylphenol)/poly(methyl acrylate) and poly(vinylphenol)/poly(methyl methacrylate) blends: Hydrogen bonding, miscibility, and blending effects on molecular motions as studied by carbon-13 CP/MAS NMR. *Macromolecules* **1991**, *24*, 5756–5762.
7. Li, D.; Brisson, J. DMTA and FTIR Investigation of the Phase Behavior of Poly(methyl methacrylate)–Poly(4-vinylphenol) Blends. *Macromolecules* **1996**, *29*, 868–874.
8. Li, D.; Brisson, J. Hydrogen bonds in poly(methyl methacrylate)-poly(4-vinyl phenol) blends: 1. Quantitative analysis using *FT*i.r. spectroscopy. *Polymer* **1998**, *39*, 793–800.
9. Dong, J.; Ozaki, Y. FTIR and FT-Raman Studies of Partially Miscible Poly(methyl methacrylate)/Poly(4-vinylphenol) Blends in Solid States. *Macromolecules* **1997**, *30*, 286–292.
10. Goh, S.H.; Siow, K.S. Miscibility of poly(p-vinyl phenol) with polymethacrylates. *Polym. Bull.* **1987**, *17*, 453–457.
11. Serman, S.J.; Painter, P.C.; Coleman, M.M. Studies of the phase behaviour of poly(vinyl phenol)-poly(n-alkyl methacrylate) blends. *Polymer* **1991**, *32*, 1049–1058.
12. Lin, C.L.; Chen, W.C.; Liao, C.S.; Su, Y.C.; Huang, C.F.; Kuo, S.W.; Chang, F.C. Sequence Distribution and Polydispersity Index Affect the Hydrogen-Bonding Strength of Poly(vinylphenol-*co*-methyl methacrylate) Copolymers. *Macromolecules* **2005**, *38*, 6435–6444.
13. Kuo, S.W.; Chang, F.C. Miscibility and Hydrogen Bonding in Blends of Poly(vinylphenol-*co*-methyl methacrylate) with Poly(ethylene oxide). *Macromolecules* **2001**, *34*, 4089–4097.
14. Chen, W.C.; Kuo, S.W.; Jeng, U.S.; Chang, F.C. Self-Assembly through Competitive Interactions of Miscible Diblock Copolymer/Homopolymer Blends: Poly(vinylphenol-*b*-methyl methacrylate)/Poly(vinylpyrrolidone) Blend. *Macromolecules* **2008**, *41*, 1401–1410.
15. Kuo, S.W. Hydrogen bond-mediated self-assembly and supramolecular structures of diblock copolymer mixtures. *Polym. Int.* **2009**, *58*, 455–464.

16. Ni, Y.P.; Becquart, F.; Chen, J.D.; Taha, M. Polyurea–Urethane Supramolecular Thermo-Reversible Networks. *Macromolecules* **2013**, *46*, 1066–1074.
17. Wang, S.J.; Xu, Y.S.; Yang, S.; Chen, E.Q. Phase Behavior of a Hydrogen-Bonded Polymer with Lamella-to-Cylinder Transition: Complex of Poly(4-vinylpyridine) and Small Dendritic Benzoic Acid Derivative. *Macromolecules* **2012**, *45*, 8760–8769.
18. Kuo, S.W.; Chen, C.J. Functional Polystyrene Derivatives Influence the Miscibility and Helical Peptide Secondary Structures of Poly(γ-benzyl L-glutamate). *Macromolecules* **2012**, *45*, 2442–2452.
19. Painter, P.C.; Veytsman, B.; Kumar, S.; Shenoy, S.; Graf, J.F.; Xu, Y.; Coleman, M.M. Intramolecular Screening Effects in Polymer Mixtures. 1. Hydrogen-Bonded Polymer Blends. *Macromolecules* **1997**, *30*, 932–942.
20. Pehlert, G.J.; Painter, P.C.; Veytsman, B.; Coleman, M.M. Functional Group Accessibility in Hydrogen-Bonded Polymer Blends. 2. Miscibility Map of 2,3-Dimethylbutadiene-*stat*-vinylphenol Blends with Ethylene-*stat*-vinyl acetate. *Macromolecules* **1997**, *30*, 3671–3677.
21. Pehlert, G.J.; Painter, P.C.; Coleman, M.M. Functional Group Accessibility in Hydrogen-Bonded Polymer Blends. 3. Steric Shielding Effects. *Macromolecules* **1998**, *31*, 8423–8424.
22. Coleman, M.M.; Xu, Y.; Painter, P.C. Compositional heterogeneities in hydrogen-bonded polymer blends: infrared spectroscopic results. *Macromolecules* **1994**, *27*, 127–134.
23. Pruthtikul, R.; Coleman, M.; Painter, P.C.; Tan, N.B. Screening Effects in Solutions of a Hyperbranched, Dendrimer-Like Polyester. *Macromolecules* **2001**, *34*, 4145–4150.
24. Huang, C.F.; Kuo, S.W.; Lin, H.C.; Chen, J.K.; Chen, Y.K.; Xu, H.Y.; Chang, F.C. Thermal properties, miscibility and specific interactions in comparison of linear and star poly(methyl methacrylate) blend with phenolic. *Polymer* **2004**, *45*, 5913–5921.
25. Huang, C.F.; Kuo, S.W.; Lin, F.L.; Huang, W.J.; Wang, C.F.; Chen, W.Y.; Chang, F.C. Influence of PMMA-Chain-End Tethered Polyhedral Oligomeric Silsesquioxanes on the Miscibility and Specific Interaction with Phenolic Blends. *Macromolecules* **2006**, *39*, 300–308.
26. Kuo, S.W.; Chang, F.C. POSS related polymer nanocomposites. *Prog. Polym. Sci.* **2011**, *36*, 1649–1696.
27. Zhang, W.A.; Muller, A.H.E. Architecture, self-assembly and properties of well-defined hybrid polymers based on polyhedral oligomeric silsequioxane (POSS). *Prog. Polym. Sci.* **2013**, *38*, 1121–1162.
28. Tanaka, K.; Chujo, Y. Unique properties of amphiphilic POSS and their applications. *Polym. J.* **2013**, *45*, 247–254.
29. Xu, H.; Kuo, S.W.; Lee, J.S.; Chang, F.C. Glass transition temperatures of poly(hydroxystyrene-*co*-vinylpyrrolidone-*co*-isobutylstyryl polyhedral oligosilsesquioxanes). *Polymer* **2002**, *43*, 5117–5124.
30. Lee, Y.J.; Huang, J.M.; Kuo, S.W.; Lu, J.S.; Chang, F.C. Polyimide and polyhedral oligomeric silsesquioxane nanocomposites for low-dielectric applications. *Polymer* **2005**, *46*, 173–181.
31. Lin, H.C.; Kuo, S.W.; Huang, C.F.; Chang, F.C. Thermal and Surface Properties of Phenolic Nanocomposites Containing Octaphenol Polyhedral Oligomeric Silsesquioxane. *Macromol. Rapid Commun.* **2006**, *27*, 537–541.

32. Zhang, W.C.; Li, X.M.; Yang, R.J. Blowing-out effect and temperature profile in condensed phase in flame retarding epoxy resins by phosphorus-containing oligomeric silsesquioxane. *Polym. Adv. Tech.* **2013**, *24*, 951–961.
33. Li, Y.W.; Wang, Z.; Zheng, J.K.; Su, H.; Lin, F.; Guo, K.; Feng, X.; Wesdemiotis, C.; Becker, M.L.; Cheng, S.Z.D.; Zhang, W.B. Cascading One-Pot Synthesis of Single-Tailed and Asymmetric Multitailed Giant Surfactants. *ACS Macro Lett.* **2013**, *2*, 1026–1032.
34. Yue, K.; Liu, C.; Guo, K.; Yu, X.F.; Huang, M.J.; Li, Y.W.; Wesdemiotis, C.; Cheng, S.Z.D.; Zhang, W.B. Sequential "Click" Approach to Polyhedral Oligomeric Silsesquioxane-Based Shape Amphiphiles. *Macromolecules* **2012**, *45*, 8126–8134.
35. Hu, W.H.; Huang, K.W.; Chiou, C.W.; Kuo, S.W. Complementary Multiple Hydrogen Bonding Interactions Induce the Self-Assembly of Supramolecular Structures from Heteronucleobase-Functionalized Benzoxazine and Polyhedral Oligomeric Silsesquioxane Nanoparticles. *Macromolecules* **2012**, *45*, 9020–9028.
36. Kuo, S.W.; Chen, C.J. Using Hydrogen-Bonding Interactions To Control the Peptide Secondary Structures and Miscibility Behavior of Poly(L-glutamate)s with Phenolic Resin. *Macromolecules* **2011**, *44*, 7315–7326.
37. Li, J.G.; Lin, Y.D.; Kuo, S.W. From Microphase Separation to Self-Organized Mesoporous Phenolic Resin through Competitive Hydrogen Bonding with Double-Crystalline Diblock Copolymers of Poly(ethylene oxide-*b*-ε-caprolactone). *Macromolecules* **2011**, *44*, 9295–9309.
38. Li, J.G.; Chu, W.C.; Jeng, U.S.; Kuo, S.W. *In Situ* Monitoring of the Reaction-Induced Self-Assembly of Phenolic Resin Templated by Diblock Copolymers. *Macromol. Chem. Phys.* **2013**, *214*, 2115–2123.
39. Hirai, T.; Leolukman, M.; Jin, S.; Goseki, R.; Ishida, Y.; Kakimoto, M.; Hayakawa, T.; Ree, M.; Gopalan, P. Hierarchical Self-Assembled Structures from POSS-Containing Block Copolymers Synthesized by Living Anionic Polymerization. *Macromolecules* **2009**, *42*, 8835–8843.
40. Ishida, Y.; Hira, T.; Goseki, R.; Tokita, M.; Kakimoto, A.; Hayakawa, T. Synthesis and self-assembly of thermotropic block copolymer with long alkyl tethered cage silsesquioxane in the side chain. *J. Polym. Sci. A Polym. Chem.* **2011**, *49*, 2653–2664.
41. Wu, Y.C.; Kuo, S.W. Synthesis and characterization of polyhedral oligomeric silsesquioxane (POSS) with multifunctional benzoxazine groups through click chemistry. *Polymer* **2010**, *51*, 3948–3955.
42. Huang, K.W.; Kuo, S.W. High-Performance Polybenzoxazine Nanocomposites Containing Multifunctional POSS Cores Presenting Vinyl-Terminated Benzoxazine Groups. *Macromol. Chem. Phys.* **2010**, *211*, 2301–2311.
43. Kuo, S.W.; Chan, S.C.; Chang, F.C. Miscibility enhancement on the immiscible binary blend of poly(vinyl acetate) and poly(vinyl pyrrolidone) with bisphenol A. *Polymer* **2002**, *43*, 3653–3660.
44. Kwei, T.K. The effect of hydrogen bonding on the glass transition temperatures of polymer mixtures. *J. Polym. Sci. Polym. Lett. Ed.* **1984**, *22*, 307–313.
45. Kuo, S.W.; Chan, S.C.; Chang, F.C. The effect of hydrogen bonding on the glass transition temperatures of polymer mixtures. *Macromolecules* **2003**, *36*, 6653–6661.
46. Kuo, S.W.; Chang, F.C. Miscibility Behavior and Specific Interaction of Phenolic Resin with Poly(acetoxystyrene) Blends. *Macromol. Chem. Phys.* **2002**, *203*, 868–878.

47. Lee, Y.J.; Kuo, S.W.; Huang, W.J.; Lee, H.Y.; Chang, F.C. Miscibility, specific interactions, and self-assembly behavior of phenolic/polyhedral oligomeric silsesquioxane hybrids. *J. Polym. Sci. Polym. Phys.* **2004**, *42*, 1127–1136.
48. Kuo, S.W.; Lin, H.C.; Huang, W.J.; Huang, C.F.; Chang, F.C. Hydrogen bonding interactions and miscibility between phenolic resin and octa(acetoxystyryl) polyhedral oligomeric silsesquioxane (AS-POSS) nanocomposites. *J. Polym. Sci. Polym. Phys.* **2006**, *44*, 673–686.
49. Jin, S.; Hira, T.; Ahn, B.; Rho, Y.; Kim, K.W.; Kakimoto, M.A.; Gopalan, P.; Hayakawa, T.; Ree, M. Synchrotron Grazing Incidence X-ray Scattering Study of the Morphological Structures in Thin Films of a Polymethacrylate Diblock Copolymer Bearing POSS Moieties. *J. Phys. Chem. B* **2010**, *114*, 8033–8042.
50. Chen, Y.; Kang, E.T. New approach to nanocomposites of polyimides containing polyhedral oligomeric silsesquioxane for dielectric applications. *Mater. Lett.* **2004**, *58*, 3716–3719.
51. Li, X.D.; Goh, S.H.; Zheng, J.W. Specific interactions and phase behavior of poly(2-vinylpridine)/bisphenol blends. *J. Appl. Polym. Sci.* **2003**, *87*, 1137–1143.
52. Chen, W.C.; Kuo, S.W.; Lu, C.H.; Chang, F.C. Self-Assembly Structures through Competitive Interactions of Crystalline–Amorphous Diblock Copolymer/Homopolymer Blends: Poly(ε-caprolactone-b-4-vinyl pyridine)/Poly(vinyl phenol). *Macromolecules* **2009**, *42*, 3580–3590.